COMMUNICATION

Check for updates

Highly active and noble-metal-alternative hydrogenation catalysts prepared by dealloying Ni–Si intermetallic compounds†

Wiyanti F. Simanullang,[a] Hiroshi Itahara, [ID][b] Naoko Takahashi,[b] Satoru Kosaka,[b] Ken-ichi Shimizu [ID][ac] and Shinya Furukawa [ID]*[ac]

Noble-metal-alternative Ni–Si catalysts more active than Pd in the hydrogen storage reaction were developed using a unique procedure, *i.e.*, surface dealloying with hydrofluoric acid treatment. The combination of the structural analysis and the DFT calculation revealed a specific active site structure, a Ni cluster embedded in a SiO₂ matrix, and its unprecedented role in the molecular conversion.

Hydrogenation is one of the most important chemical transformations in various systems such as industrial processes, pharmaceutical synthesis, and hydrogen storage.[1] Noble metals such as Pt and Pd have been used as efficient catalysts for the hydrogenation of unsaturated hydrocarbons. However, because these noble metals are rare, unevenly distributed, and extremely expensive, the development of alternatives is strongly desired.[2] As a non-noble metal, Ni has been used in various hydrogenation reactions involving, for example, aldehydes,[3] nitroarenes,[4] aromatics,[5] and unsaturated fatty acids.[6] However, severe reaction conditions such as high temperatures and hydrogen pressures are typically needed to attain sufficient reaction rates. Therefore, a drastic enhancement in the catalytic activity of Ni is a challenging but attractive approach to develop an efficient alternative to noble-metal catalysts.

Intermetallic compounds are receiving increasing attention as attractive catalyst materials because of their specific crystal structures, ordered atomic arrangements, and unique electronic states.[7] Emerging research topics in this field include the use of intermetallic compounds as a platform to develop more efficient reaction environments *via* a chemical treatment.[8–11] Two different well-ordered and atomically dispersed metal elements can be transformed into a composite with unconventional active sites *via* an appropriate chemical treatment.

In this study, we applied a ''surface dealloying'' methodology to a series of Ni-based intermetallic compounds such that only the surface structure was chemically modified, whereas the bulk structure was retained. During an attempt to develop an efficient hydrogenation catalyst based on surface dealloying, we discovered that some Ni–Si intermetallic compounds treated with a diluted aqueous solution of hydrofluoric acid (HF) exhibited outstanding catalytic performances in the hydrogenation of unsaturated hydrocarbons. In addition, a combination of X-ray photoelectron spectroscopy (XPS), scanning transmission electron microscopy (STEM) analysis, and density functional theory (DFT) studies suggested that Ni clusters partially embedded in the SiO₂ matrix acted as highly active hydrogenation sites. Herein, we report a promising noble-metal-alternative material based on Ni with earth-abundant Si and a novel concept in catalyst preparation.

The procedure for catalyst preparation was very simple: a series of Ni-based intermetallic compounds prepared by arc melting (Ni₃Si, Ni₂Si, NiSi, NiSi₂, Ni₃Al, Ni₃Ge, and Ni₃Sn as fine powders; X-ray diffraction (XRD) patterns are shown in Fig. S1, ESI†) was added to a vigorously stirred aqueous solution of HF (typically 1.0 M) at 25 °C in air and the resultant solution was allowed to stand for 15 min, followed by three washings with deionized water. The thus-prepared catalysts were pre-reduced under flowing hydrogen at 400 °C and tested in the hydrogenation of ethylene as a model reaction (Table S1, ESI†). Fig. 1 shows the catalytic activities of these samples relative to that of pure Ni. Among the various materials, Ni₃Si and NiSi₂ showed remarkably high catalytic activities compared with Ni powder (a 20-fold higher turnover frequency (TOF) and reaction rate, respectively) and Ni/SiO₂ (Ni nanoparticles supported on silica gel: 7–10 nm, Fig. S2, ESI†). Ni₃Al–HF, which is a RANEY® Ni analog, did not demonstrate such a large enhancement. The catalytic activity did not change when pure Ni was treated with HF. No reaction occurred when Ni₃Ge–HF or Ni₃Sn–HF was used. These results indicate that the observed high catalytic activity is specific to the combination of Ni and Si.

We next characterized the structures of the Ni–Si catalysts before and after the HF treatment. The XRD patterns (Fig. S3, ESI†) and

[a] *Institute for Catalysis, Hokkaido University, N21 W10, Kita-ku, Sapporo, 001-0021, Japan. E-mail: furukawa@cat.hokudai.ac.jp*

[b] *Toyota Central Research & Development Labs, Inc., 41-1 Yokomichi Nagakute, Aichi 480-1192, Japan*

[c] *Elements Strategy Initiative for Catalysts and Batteries, Kyoto University, Katsura, Kyoto 615-8520, Japan*

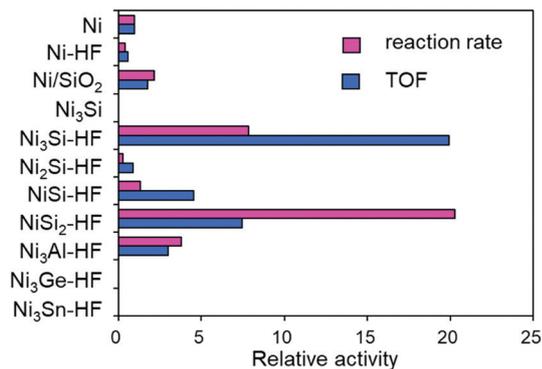† Electronic supplementary information (ESI) available. See DOI: 10.1039/c9cc07862b

Fig. 1 Relative catalytic activities of Ni-based materials in ethylene hydrogenation at 70 °C. Specific reaction rate per gram catalyst and TOF relative to those of pure Ni as unity are shown.

X-ray adsorption spectra (Fig. S4, ESI†) of the catalysts after HF treatment were almost identical to those of the untreated materials, indicating that the bulk structure was retained after the HF treatment. However, CO adsorption experiments revealed that the Ni dispersion substantially increased from zero depending on the concentration of HF (Fig. S5a, ESI†). These results suggest that Si species at the surface region were preferentially removed by the HF treatment, thus forming a Ni-rich surface. With increasing HF concentration, the Ni dispersion and the reaction rate initially increased and then plateaued (Fig. S5a and b, ESI†). The TOF reached a certain maximum at $1.0 \leq [HF] \leq 2.0$ M for each Ni–Si intermetallic compound (Fig. S5c, ESI†). Details of the effect of [HF] are summarized in the ESI† (p. S25). SEM images of $NiSi_2$ and $NiSi_2$–HF revealed that the particle size and morphology did not change, while the surface became rough (Fig. S6, ESI†). This is consistent with the bulk and surface structures being retained and chemically modified, respectively.

Next, we tested the catalytic activities of Ni_3Si–HF and $NiSi_2$–HF in the hydrogenation of various unsaturated hydrocarbons such as acetylene, benzene, and toluene (Table S2, ESI†). Acetylene hydrogenation is the key process in purifying ethylene before polymerization.[12] Benzene and toluene have attracted attention as promising hydrogen carriers;[13,14] therefore, the development of an efficient catalyst for aromatic hydrogenation using non-noble metals is strongly desired. Fig. 2 shows the relative catalytic activity of these catalysts. In addition to their excellent ethylene hydrogenation performance, Ni_3Si–HF and $NiSi_2$–HF exhibited outstanding catalytic activities compared with that of Ni in acetylene hydrogenation. These catalysts also showed excellent aromatic hydrogenation performance (TOFs typically 10 or 20 times greater than that of Ni). $NiSi_2$–HF gave the highest reaction rate in each reaction, likely because Ni was much more dispersed than in Ni_3Si–HF (Fig. S5b, ESI†).

Given the aforementioned high reaction rates, we further studied the catalytic activity and stability of $NiSi_2$–HF in aromatic hydrogenation under optimized conditions.

Fig. 3 shows the change in reactant conversion in the hydrogenation of benzene and toluene over $NiSi_2$–HF, Pd black, and Ni catalysts. Here note that the Ni content in $NiSi_2$–HF was 51 wt%. The pure Ni catalyst gave poor conversions less than
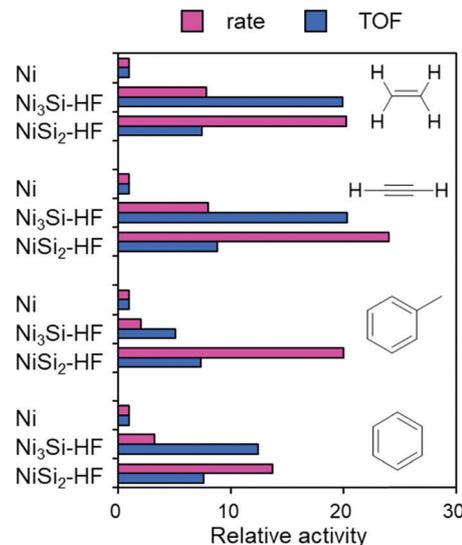

Fig. 2 Relative catalytic activities of Ni, Ni_3Si–HF, and $NiSi_2$–HF in the hydrogenation of various unsaturated hydrocarbons. The specific reaction rate per gram of catalyst and the TOF relative to those of pure Ni as unity are shown.

5% in both reactions. $NiSi_2$–HF gave excellent conversions (ca. 93% for benzene and 91% for toluene) and retained them for at least 8 h. We also tested the catalytic activity of Pd black, in which the metal was slightly more dispersed than that in $NiSi_2$–HF (Fig. 3 and Table S3, ESI†). Compared with Pd black, $NiSi_2$–HF exhibited much higher and comparable conversions of benzene and toluene, respectively. $NiSi_2$–HF also showed a 1.5-times higher TOF than Pd. The turnover number reached 5185 after 8 h on stream, which was much higher than that of Pd (3038, Table S3, ESI†). These results highlight that $NiSi_2$–HF is a promising noble-metal-alternative material for hydrogen storage applications.

To consider the surface states of HF-treated catalysts, we conducted XPS analyses. Fig. 4a and b shows the Ni $2p_{3/2}$ and Si 2p XPS spectra of $NiSi_2$ before and after the HF treatment and the subsequent H_2 reduction.

The spectrum of $NiSi_2$ shows emission peaks at 854.6 and 100.3 eV in the Ni $2p_{3/2}$ and Si 2p regions, respectively,
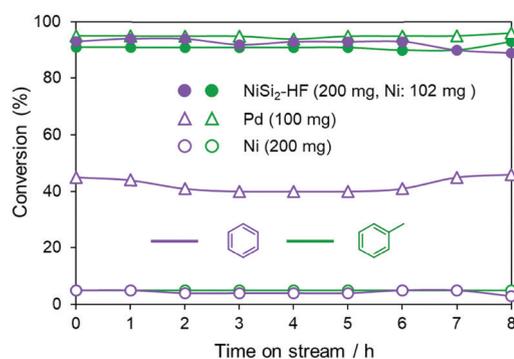

Fig. 3 Change in reactant conversion in the hydrogenation of benzene and toluene over $NiSi_2$–HF, Pd black, and Ni catalysts at 150 °C. The selectivity toward cyclohexane or methylcyclohexane was 100% for each catalyst.

consistent with reported values for zero-valent Ni and Si of $NiSi_2$.[15] An intense peak assignable to SiO_2 was also observed at 103.6 eV,[15] suggesting that the Si species at the surface were partially oxidized (Fig. 4c, left). After the HF treatment, the Ni $2p_{3/2}$ peak intensity increased, whereas the Si 2p intensity decreased, consistent with the removal of surface Si and an increase in Ni dispersion, as previously mentioned. Moreover, $Si^{(0)}$ species disappeared and two Ni species were newly observed at 852.8 and 856.0 eV, which were assignable to elemental Ni[15] and NiO,[16] respectively. These results indicate that Ni was separated from the parent intermetallic phase during the dealloying process by HF and that part of the Si remained as SiO_2 (Fig. 4c). The presence of NiO after H_2 reduction implies that some Ni species are fully embedded in the resulting SiO_2 matrix, which hardly comes into contact with gaseous H_2. Fig. 4d shows the bright field-STEM image of $NiSi_2$–HF, where a specific layered structure is indeed observed (see also Fig. S7 for several viewpoints, ESI†). The elemental map in this field (Fig. S8, ESI†) revealed that each layer consisted of a number of small Ni clusters (2–5 nm) embedded in SiO_2, SiO_2, and $NiSi_2$, which demonstrates the structural model shown in Fig. 4c. Thus, a specific surface structure consisting of Ni–SiO_2 composites was obtained by applying the surface dealloying protocol. Given that Ni/SiO_2 showed a TOF similar to that of bulk Ni, the high catalytic activities of Ni–Si–HF cannot be explained by a simple contact between the Ni and SiO_2, as observed for supported nanoparticles. A similar trend in peak intensity was also observed for the XPS of Ni_3Si and Ni_3Si–HF (Fig. S9, ESI†). However, for Ni_3Si, the surface of the parent Ni_3Si was already segregated: the hard X-ray photoelectron spectra of Ni_3Si revealed that the as-prepared Ni_3Si had a thick SiO_2 layer (>20 nm, Fig. S10, ESI†) at the surface. The presence of this thick SiO_2 layer at the catalyst surface can explain why the untreated Ni_3Si was inactive. The Ni_3Si phase itself is known to be active toward hydrogenation:[17,18] we recently reported that Ni_3Si fine powder prepared by sodium melt synthesis (Ni_3Si-p) exhibited high phase purity and a much less oxidized surface; hence, it exhibited a higher TOF than Ni in ethylene hydrogenation.[17] However, emphasis should be placed on the observation that Ni_3Si–HF still afforded a TOF more than two times that of Ni_3Si-p under the same reaction conditions (Fig. S12, ESI†).

To clarify the role of surface structures in the observed enhancement in hydrogenation ability, we performed DFT calculations for the relevant Ni-based materials. The flat surfaces of Ni(111) and Ni_3Si(111) were considered the standard active surfaces of Ni and Ni_3Si-p, respectively. On the basis of the XPS and STEM analysis results, we considered a Ni cluster partially embedded in an SiO_2 matrix to be the active site of Ni–Si–HF (hereafter, Ni@SiO_2). In this study, we modeled a Ni_{20} cluster as a small truncated octahedron with or without a surrounding SiO_2 matrix (Fig. S12, ESI†). For the Ni@SiO_2 model, a cavity was made in a SiO_2 framework with an appropriate size and OH terminations for the embedded Ni_{20} cluster to fit within the cavity. The closest contact between Ni and the lattice oxygen or OH groups ranged within 1.86–2.16 Å in the optimized structure (Fig. S12d, ESI†), which would provide moderate steric restriction or strain to the Ni cluster. Fig. 5 shows the activation energies associated with hydrogen attack at ethylene adsorbed onto the relevant Ni-based surfaces (detailed structures are shown in Fig. S13, ESI†). The Ni_{20} clusters gave an activation energy of 0.80 eV, which is similar to that on the Ni(111) surface (0.76 eV). This similarity indicates that the metal size weakly affects the reactivity, as reported in the literature.[19] The Ni_3Si(111) surface
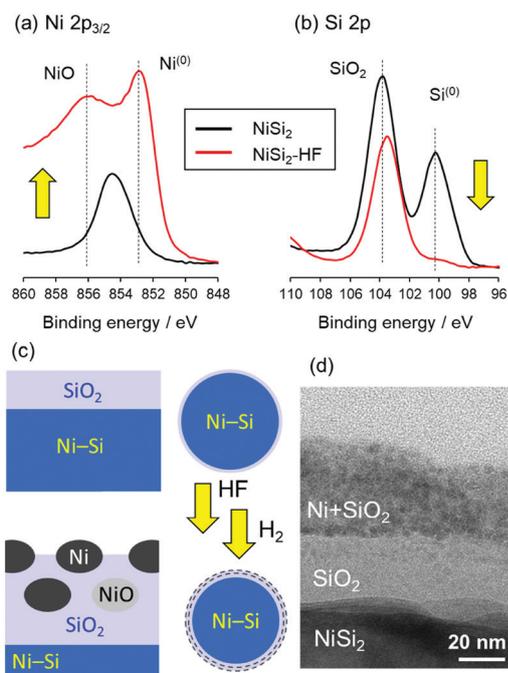

Fig. 4 (a) Ni $2p_{3/2}$ and (b) Si 2p XPS of $NiSi_2$ before and after HF treatment. (c) Plausible change in the surface structure upon HF treatment and H_2 reduction. (d) The bright-field-STEM image of the surface region of $NiSi_2$–HF in the cross-section.
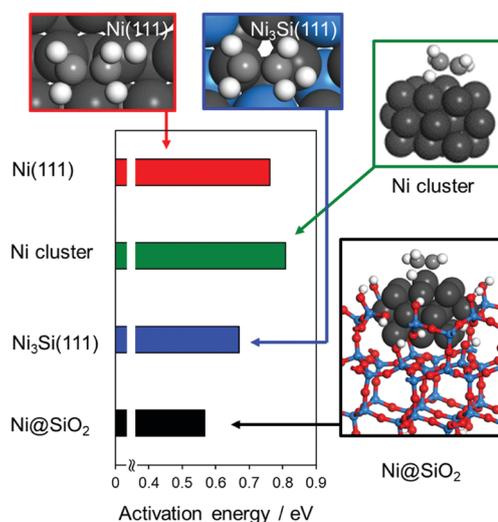

Fig. 5 Activation energies of the hydrogen attack at ethylene on Ni(111), Ni_3Si(111), a Ni_{20} cluster, and a Ni_{20} cluster embedded in an SiO_2 matrix, as calculated by DFT. Transition-state structures are also shown.

showed a lower activation energy of 0.67 eV, consistent with the catalytic activity of Ni₃Si-p being higher than that of Ni. The lowest activation energy of 0.56 eV was observed for Ni@SiO$_2$, where a substantial decrease in the energy barrier (0.24 eV) with the aid of the SiO$_2$ matrix was observed. Thus, our calculation results could explain the experimental activity trend: Ni₃Si–HF (Ni@SiO$_2$) > Ni₃Si-p > Ni ≈ Ni/SiO$_2$. The substantial stabilization observed for Ni@SiO$_2$ was attributed to the specific structure of the transition state: the active site of the Ni-atom-absorbing ethylene was uplifted compared with that of the free Ni cluster (Fig. 5 and Fig. S12, ESI†). Hydrogen attack to the upper-lying alkenyl carbon can be facilitated over the uplifted active sites, thereby stabilizing the transition state. This specific structure likely originates from the steric restriction provided by the surrounding SiO$_2$ matrix: because the lateral displacement of Ni atoms is restricted, the displacement to the vertical direction could be amplified.

We also focused on the effect of the SiO$_2$ matrix on the electronic state of Ni. However, the difference in the atomic charge of Ni between Ni$_{20}$ and Ni@SiO$_2$ was negligible (Table S4, ESI†). This result is consistent with the XPS analysis results: the surface Ni of Ni–Si–HF showed a binding energy identical to that of elemental Ni. The metal–support interaction is known to be weak for SiO$_2$, unlike that for other common oxide supports such as TiO$_2$ and Al$_2$O$_3$.[20] This character may be one of the reasons why only Ni–Si–HF among the various investigated Ni–M–HF showed a specific improvement.

The Ni@SiO$_2$ model we used is just one of the possible model structures. However, the important consideration is that our DFT model suggested an unprecedented strain effect on the catalytic activity. In addition, such a highly active reaction site could be constructed using the surface dealloying protocol, which is simple and easy. The obtained insights and catalyst design could also be applicable for supported nanoparticulate catalysts, which are expected to be much more efficient. We are currently focusing on developing supported Ni@SiO$_2$ catalysts and will report another efficient system in the near future. Thus, our findings propose an innovative concept for catalyst design and would open a novel trend in catalysis research.

In summary, we prepared highly efficient catalysts for hydrogenation based on a novel concept of catalyst design, i.e., surface dealloying of intermetallic compounds. Compared with the conventional Ni catalysts, Ni₃Si and NiSi$_2$ treated with HF function as remarkably active hydrogenation catalysts for several unsaturated hydrocarbons, where a 10- to 20-fold increase in catalytic activity was achieved. NiSi$_2$–HF exhibits excellent catalytic activity and stability in the hydrogenation of benzene and toluene. Emphasis should be placed on this catalyst being even more active than Pd in aromatic hydrogenation, indicating that the developed catalysts are efficient noble-metal-alternative materials for hydrogen storage and transport. The surface of Ni–Si is dealloyed by HF to form Ni–SiO$_2$ composites, where Ni clusters are embedded in the SiO$_2$ matrix. Steric restriction imposed on the Ni cluster by the SiO$_2$ matrix enables stabilization of the hydrogenation transition state, which substantially lowers the activation barrier. The insights obtained in this study not only provide an efficient catalytic system but would also open a novel trend in catalyst design.

Conflicts of interest

There are no conflicts to declare.

References

1 N. B. Johnson, I. C. Lennon, P. H. Moran and J. A. Ramsden, *Acc. Chem. Res.*, 2007, **40**, 1291–1299.
2 P. J. Chirik, *Catalysis without Precious Metals*, Wiley-VCH Verlag GmbH & Co. KGaA, 2010, pp. 83–110, DOI: 10.1002/9783527631582.ch4.
3 A. Reinsdorf, W. Korth, A. Jess, M. Terock, F. Klasovsky and R. Franke, *ChemCatChem*, 2016, **8**, 3592–3599.
4 R. S. Downing, P. J. Kunkeler and H. vanBekkum, *Catal. Today*, 1997, **37**, 121–136.
5 P. G. Savva, K. Goundani, J. Vakros, K. Bourikas, C. Fountzoula, D. Vattis, A. Lycourghiotis and C. Kordulis, *Appl. Catal., B*, 2008, **79**, 199–207.
6 D. Jovanovic, R. Radovic, L. Mares, M. Stankovic and B. Markovic, *Catal. Today*, 1998, **43**, 21–28.
7 S. Furukawa and T. Komatsu, *ACS Catal.*, 2017, **7**, 735–765.
8 M. Armbrüster, R. Schlögl and Y. Grin, *Sci. Technol. Adv. Mater.*, 2014, **15**, 034803.
9 S. Kameoka, S. Wakabayashi, E. Abe and A. P. Tsai, *Catal. Lett.*, 2016, **146**, 1309–1316.
10 S. Furukawa, A. Tsuchiya, Y. Kojima, M. Endo and T. Komatsu, *Chem. Lett.*, 2016, **45**, 158–160.
11 S. Shoji, X. Peng, T. Imai, P. S. Murphin Kumar, K. Higuchi, Y. Yamamoto, T. Tokunaga, S. Arai, S. Ueda, A. Hashimoto, N. Tsubaki, M. Miyauchi, T. Fujita and H. Abe, *Chem. Sci.*, 2019, **10**, 3701–3705.
12 A. Borodzinki, *Catal. Rev.*, 2006, **48**, 91–144.
13 R. B. Biniwale, S. Rayalu, S. Devotta and M. Ichikawa, *Int. J. Hydrogen Energy*, 2008, **33**, 360–365.
14 Y. Okada, E. Sasaki, E. Watanabe, S. Hyodo and H. Nishijima, *Int. J. Hydrogen Energy*, 2006, **31**, 1348–1356.
15 Y. Cao, L. Nyborg and U. Jelvestam, *Surf. Interface Anal.*, 2009, **41**, 471–483.
16 M. A. Peck and M. A. Langell, *Chem. Mater.*, 2012, **24**, 4483–4490.
17 H. Itahara, W. F. Simanullang, N. Takahashi, S. Kosaka and S. Furukawa, *Inorg. Chem.*, 2019, **58**, 5406–5409.
18 P. Ryabchuk, G. Agostini, M.-M. Pohl, H. Lund, A. Agapova, H. Junge, K. Junge and M. Beller, *Sci. Adv.*, 2018, **4**, eaat0761.
19 C.-K. Tsung, J. N. Kuhn, W. Huang, C. Aliaga, L.-I. Hung, G. A. Somorjai and P. Yang, *J. Am. Chem. Soc.*, 2009, **131**, 5816–5822.
20 S. Furukawa, K. Ozawa and T. Komatsu, *RSC Adv.*, 2013, **3**, 23269–23277.